In vivo liver tracking with a high volume rate 4D ultrasound scanner and a 2D matrix array probe

Muyinatu A. Lediju Bell[1,2], Brett C Byram[2], Emma J Harris[1], Philip M Evans[1], Jeffrey C Bamber[1]

[1]Joint Department of Physics, Institute of Cancer Research and Royal Marsden Hospital, Sutton, Surrey SM2 5NG, UK

[2]Department of Biomedical Engineering, Duke University, Durham, NC 27708, USA

E-mail: muyinatu.lediju@duke.edu

Abstract. The effectiveness of Intensity Modulated Radiation Therapy (IMRT) is compromised by involuntary motion (e.g. respiration, cardiac activity). The feasibility of processing ultrasound echo data to automatically estimate 3D liver motion for real-time IMRT guidance was previously demonstrated, but performance was limited by an acquisition speed of 2 volumes per second due to hardware restrictions of a mechanical linear array probe. Utilizing a 2D matrix array probe with parallel receive beamforming offered increased acquisition speeds and an opportunity to investigate the benefits of higher volume rates. *In vivo* livers of three volunteers were scanned with and without respiratory motion at volume rates of 24 and 48 Hz, respectively. Respiration was suspended via voluntary breath hold. Correlation-based, phase-sensitive 3D speckle tracking was applied to consecutively-acquired volumes of echo data. Volumes were omitted at fixed intervals and 3D speckle tracking was reapplied to study the effect of lower scan rates. Results revealed periodic motion that corresponded with the heart rate or breathing cycle, in the absence or presence of respiration, respectively. For cardiac-induced motion, volume rates for adequate tracking ranged from 8-12 Hz and was limited by frequency discrepancies between tracking estimates from higher- and lower-frequency scan rates. Thus, the scan rate of volume data acquired without respiration was limited by the need to sample the frequency induced by the beating heart. In respiratory-dominated motion, volume rate limits ranged from 4-12 Hz, interpretable from the root mean squared deviation (RMSD) from tracking estimates at 24 Hz. While higher volume rates yielded RMSD values less than 1 mm in most cases, lower volume rates yielded RMSD values on the order of 2-6 mm.

Keywords: ultrasound, 3D speckle tracking, real-time image-guided radiotherapy (IGRT), motion-compensated radiotherapy

1. Introduction

Intensity modulated radiation therapy (IMRT) is a targeted treatment that shapes the treatment beam profile to deliver greater radiation doses to cancerous tumors and less to surrounding tissues. Involuntary motion during IMRT (e.g. respiration, cardiac activity) compromises effectiveness, due to the risk of geometric miss. The current state of estimating liver motion for radiotherapy treatment planning is to acquire x-ray computerized tomography (CT) scans of the liver for a predetermined time period, prior to treatment. The resulting information is used to create a target volume that administers greater radiation doses to all places where the tumor has moved, an approach inherently damaging to non-cancerous tissue (Balter et al. 1996). A more detailed assessment of tumor displacement could lead to reduced planning target volumes (PTVs) and thereby limit damage to normal healthy tissue.

Liver motion that occurs over the time period of days is referred to as interfraction motion, whereas intrafraction motion occurs during the course of a 30-min. treatment session. The latter type of motion is the focus of this study, where mean peak-to-trough displacements span 5-40 mm in the superior-inferior direction under normal respiratory conditions (Davies et al. 1994, Suramo et al. 1984, Langen & Jones 2001). Intrafraction motion-compensation methods to reduce PTVs range from real-time fluoroscopy or CT tumor tracking to respiratory gating and controlled breathing (Case et al. 2010, Kubo & Hill 1996, Mageras & Yorke 2004, Dawson et al. 2001, Kitamura et al. 2003). Limitations of these techniques include the invasiveness of inserting fluoroscopic markers into the body (Shirato et al. 2000), additional doses to patients due to radiographic imaging (Murphy et al. 2007), irregular liver motion (von Siebenthal et al. 2007), and the exclusion of patients physically unable to withstand respiratory protocols (Mageras & Yorke 2004, Dawson et al. 2001, Eccles et al. 2006). Real-time tumor tracking with ultrasound does not suffer from these limitations.

The feasibility of using ultrasound to track tumors and guide radiation therapy has previously been studied. Bouchet et al. (2001) have shown that it is possible to reliably transform ultrasound image coordinates into treatment room coordinates, eliminating the need for probe orientation to be consistent with standard anatomical axes. Hsu et al. (2005) demonstrated that positioning a linear array ultrasound probe to obtain suitable images of treatment regions is possible without significantly affecting radiation dose distribution. Motion tracking performance with this probe did not suffer from ultrasound image noise caused by the radiotherapy linear accelerator and was not compromised by the probe pressure required to achieve reasonable acoustic contact. Multi-beam treatment plans and a mock transducer set-up during treatment planning were the respective solutions to conflicting probe and radiation beam positions and tissue deformations caused by the transducer (Hsu et al. 2005).

A mechanical rocking linear array probe was used to evaluate 3D tracking

performance in tissue-mimmicking phantoms (Harris et al. 2007, Harris et al. 2010) and *in vivo* livers (Harris et al. 2010). However, the scanning acquisition rate was limited to 2 volumes per second (2 Hz), due to hardware restrictions of the mechanical probe. These hardware restrictions limited speckle tracking accuracy and precision to the extent that adequate performance *in vivo* was obtained only when tracking blood vessel features (Harris et al. 2010). Further studies on phantoms indicated that poor performance in tracking fully developed speckle *in vivo* may be due to speckle decorrelation caused by elevational tissue motion (Harris et al. 2011).

The availability of a 2D matrix array probe (Frey & Chiao 2008) connected to a highly parallel receive-beam count scanner (Ustuner 2008) alleviated many of the restrictions associated with prior studies. This 4D ultrasound system was previously operated at 1000 Hz to track 3D displacements in a tissue-mimicking phantom and in *in vivo* cardiac data (Byram et al. 2010). The present study utilizes this system to assess contributions of high volume rates when tracking liver motion. Respiration is a primary contributor to intrafraction liver motion in IMRT treatment plans that allow patients to breathe normally. Likewise, liver motion due to cardiac and/or cardiovascular activity is of key importance in radiotherapy strategies that involve active breathing control and respiratory gating (Dawson et al. 2001, Wurm et al. 2006). To provide a complete analysis of appropriate volume sampling rates for ultrasonic guidance of a broad range of radiotherapy procedures, liver displacements during free breathing and voluntary breath hold are evaluated.

Motion tracking of ultrasound data is performed by applying correlation-based techniques to track an intrinsic property of ultrasound images known as speckle (Embree 1986). It is hypothesized that volume rates for adequate tracking of 3D ultrasound sector-scan data should be sufficient to restrict intervolume displacement to a few millimeters to minimize ultrasonic speckle decorrelation due to angular changes in tissue orientation (Bamber et al. 1996, Meunier 1998). Adequate volume rates are also dependent on the frequency of periodic liver motion. This study investigates if greater rates than those required by sampling theory are necessary to overcome intervolume speckle decorrelation.

2. Methods

2.1. Data Acquisition

A Siemens (Siemens Healthcare Sector, Ultrasound Business Unit, Mountain View, CA) SC2000 ultrasound scanner (Ustuner 2008) and 4Z1c matrix phased array transducer (Frey & Chiao 2008) were used to acquire 4D raw, baseband-format in-phase and quadrature (IQ) sampled echo data of *in vivo* livers from three healthy volunteers. Volunteers were scanned in the supine position on a gurney. The transducer was positioned subcostally, with its lateral direction aligned approximately with the transverse plane of the body and angled to obtain suitable views of Couinaud liver

segments IV, V, and VIII. It was affixed to the gurney via a flexible arm (Chicago Brand, model CB-50220, Fremont, CA) and custom-built probe holder. The flexible arm became rigid when locked in position once the desired orientation was achieved.

The transmit center frequency was 2.8 MHz. The transmit focus was 8 cm. The baseband IQ echo signal was sampled at 2.5 MHz. The combined effect of this level of transmit focusing and parallel receive beamforming resulted in pulse-echo lateral and elevational resolutions that were approximately 2.5 mm at the 8 cm focal depth. The lateral and elevation beam spacings were approximately 1° (i.e. 1 lateral or elevation sample is approximately 1°) .

To evaluate cardiac-induced displacements, volunteers were asked to inhale and hold their breaths during a 3-s acquisition at a volume acquisition rate of 48 Hz. This was the maximum amount of data that could be stored on the system buffer for the chosen volume configuration of 450 axial samples x 24 lateral samples x 30 elevation samples (13.8 cm x 5.8 cm x 7.2 cm sector scan). The volunteers were asked not to move but were allowed to breathe normally, while data were transferred for offline analyses and the transducer remained locked in position. Subsequently, data was acquired under normal respiratory conditions for approximately 6 s at a volume rate of 24 Hz, which was the scanner's buffer limit for the above-stated volume size and volume acquisition rate. These data were transferred for offline analyses. Synchronized ECG traces were recorded for each acquisition.

2.2. Data Analyses

Motion tracking was implemented with a phase-sensitive, normalized cross-correlation 3D speckle tracking algorithm (Wear 1987, O'Donnell et al. 1994) that was previously tested and validated with phantom experiments (Byram et al. 2010). This algorithm was applied to the acquired data, before scan conversion. A 3D kernel in one volume is specified and the vector describing the location of the best pattern match to that kernel in a consecutively-acquired volume is considered the 3D intervolume displacement of that kernel. This process was repeated for all possible kernel locations in a volume and all volumes in a data set.

The kernel size used in this study was 15 axial samples x 4 lateral samples x 4 elevation samples, which corresponds to the approximate size of two speckles at the focus. Unless otherwise stated, the search region was limited to 67 axial samples x 24 lateral samples x 26 elevation samples and was centered about the kernel location. The size of the search region was determined by the maximum size needed to find at least twice the maximum intervolume displacement observed in the three dimensions of the focal region of all data sets. The grid slopes subsample estimator (Geiman et al. 2000) was used to refine displacement estimates in the lateral and elevation dimensions.

Displacement maps were generated for axial-lateral, axial-elevation, and lateral-elevation scan planes. One pixel in a displacement map represents the displacement estimate of one kernel. Maps are available for each of the three components of

displacement and for every two sequentially-acquired volumes in a data set (i.e. as a function of time).

Motion was analyzed in a 3D region of interest (ROI) containing several pixels of displacement data from the different displacement maps. The ROI was centered about the focal depth of 8 cm and was arbitrarily chosen to measure 20 pixels (axial) x 7 pixels (lateral) x 5 pixels (elevation), which is approximately 6.2 mm x 9.8 mm x 7.0 mm, respectively. Although lateral and elevational beamwidths increase with depth, the ROI size was small enough to use the paraxial approximation to assume constant beamwidth within the ROI. Pixel displacements were converted to units of meters via the use of a conversion coordinate transformation that was correct for the center of the ROI and assumed to be apply to all pixels within the ROI. The average and standard deviations of displacements within the ROI were calculated. Average intervolume displacements were cumulatively summed to determine liver motion as a function of time. The method of tracking between consecutive volumes and cummulatively summing displacements was previously referred to as "incremental tracking", while "non-incremental tracking" was used to denote tracking with a fixed reference frame (Bamber et al. 1996, Harris et al. 2007, Harris et al. 2010). Non-incremental tracking was explored for this study, but the resulting standard deviation of displacement estimates within a ROI were significantly larger (due to larger intervolume decorrelation than that achieved with incremental tracking), and thus only the results for incremental tracking are reported.

To study the effect of decreased volume rates, relevant volumes in a data set were omitted at fixed intervals and 3D speckle tracking was re-applied. As volume rates decrease, errors due to false peaks increase (Byram et al. 2010). This type of error occurs when secondary peaks in the correlation function are higher than the true peak, yielding false estimates for a translated kernel location. When such errors occur at isolated displacement pixel locations, or for small clusters of displacement pixels, they may be detected and replaced by median filtering (Doyley et al. 2001). A 9x5 (axial x lateral) median filter was applied to displacement maps in the axial-lateral plane. Filtered and unfiltered displacement maps were analyzed as described above. All data processing was implemented with Matlab software (The Mathworks, Inc., Natick, MA).

3. Results

3.1. Cardiovascular-induced motion

A triplanar view of *in vivo* liver ultrasound data from Volunteer 1 is displayed in Fig. 1 (a). Displacement tracking of sequentially-acquired volumes of breath-hold ultrasound data resulted in relatively uniform displacement fields in most cases. This uniformity is demonstrated in Figure 1 (b-d), which shows maps of displacement in the three selected planes, for each of the three displacement components (axial, lateral, and elevation), at the same point in time (i.e. at 1.52 s in Fig. 2).

Less uniform displacement fields were observed during periods of heightened cardiac

activity (i.e. 2.35 s in Fig. 2), as evidenced in Figure 1 (e-g). These displacement maps illustrate the more pronounced spatial gradients and tissue transformations within liver, due to cardiac activity. For example, the presence of positive, negative, and zero displacements in axial displacement maps indicates deformation. Spatial gradients in lateral and elevation maps represent shearing and rotation. Similar displacement maps were mostly observed during periods of heightened cardiac activity, as dictated by the QRS complex of a synchronously-acquired ECG trace. Similar results were achieved in all volunteers.

Tracked intervolume displacements within a 3D ROI at the same location in axial, lateral, and elevation displacement maps were averaged and cumulatively summed. Average displacement as function of time is illustrated in Figure 2 (a). These displacements are attributed to cardiac activity, as data were acquired during breath hold. The corresponding ECG trace is shown in Figure 2 (b). Correlation coefficients within the ROI were above 0.98 and varied as a function of time, having lower values during periods of heightened cardiac activity, as depicted in Figure 2 (c). This trend was observed in all volunteers.

Relevant volumes were omitted and tracking was reapplied to study the effect of decreased volume rates. Displacement as a function of time for the lower volume rates is shown in Figure 3 for Volunteer 1, with the initial 48 Hz volume rate shown as a reference. The top and bottom rows of Figure 3 respectively show axial, lateral, and elevation displacement estimates before and after the median filtering of displacement maps. The mean absolute difference (MAD) between filtered and unfiltered displacement estimates ranges from 7 μm (at 48 Hz) to 70 μm (at 4 Hz) for Volunteer 1, 9 μm to 20 μm for Volunteer 2, and 6 μm to 50 μm for Volunteer 3. In some instances (e.g. compare 3(a) and 3(d)), median filtering reconciles the displacements of lower volume rates with that of higher volume rates and reveals that undersampling of the temporal displacement waveforrm is a primary source of error. Although error bars are not shown, they became larger at lower volume rates, indicative of the increased spatial variation observed within the ROI. These results demonstrate that tracking is inadequate at volume rates of 2-4 Hz, where displacement estimates deviate from that of higher volume rates and/or the periodic motion of the liver is undersampled.

Figure 4 (a) shows a histogram of correlation coefficients within the ROI used to average displacements, computed at each volume rate for Volunteer 1. Although there is some degree of overlap, the histogram reveals that lower correlation coefficients were calculated at the lower volume rates. The histogram also confirms observations that the minimum correlation coefficients for each volume rate, which occurred during periods of heightened cardiac activity, decreased with decreasing volume rates. Similar histogram trends were observed for all volunteers.

Figure 5 shows the mean correlation between tracked volumes of breath hold data within the same ROI described above, as a function of volume rate for each volunteer. Lower mean correlation coefficients at lower volume rates are observed for all volunteers.

To compare expected and measured displacement estimates for the lower

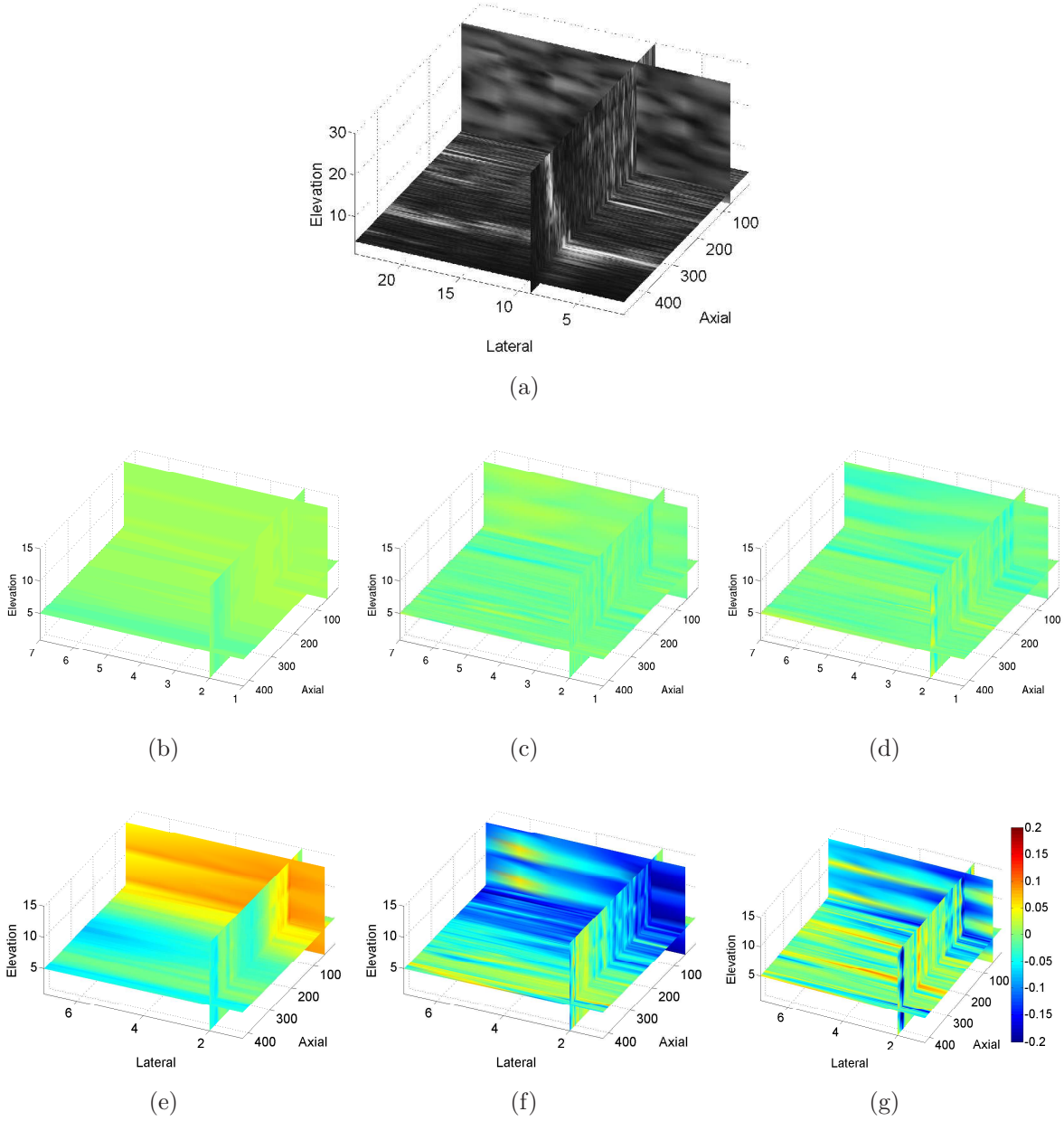

Figure 1. Triplanar views of (a) ultrasound data and corresponding (b,e) axial, (c,f) lateral, and (d,g) elevation displacement maps. The three displacement components in each row are displayed for the same point in time. The first row shows displacement fields at the 1.52-s time point in Fig. 2. The second row shows the displacement fields at the 2.35-s time point in Fig. 2. The spatial scale is pixels. The displacement scale is millimeters. One pixel in the displacement map corresponds to the displacement of one kernel of ultrasound data. The displacement maps have fewer pixels than the ultrasound image because the speckle-tracking algorithm was not applied to kernels near the boundaries of the B-mode image, where the search region extends beyond the image boundary. The search region for these images was reduced to 61 axial samples x 18 lateral samples x 26 elevation samples to show more lateral and elevational extent in the displacement maps. These displacement maps were not median filtered.

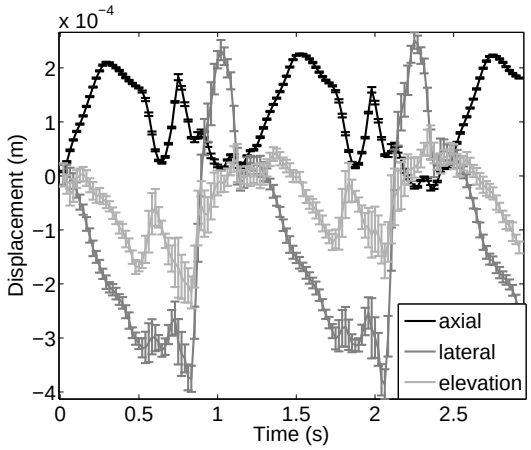

(a)

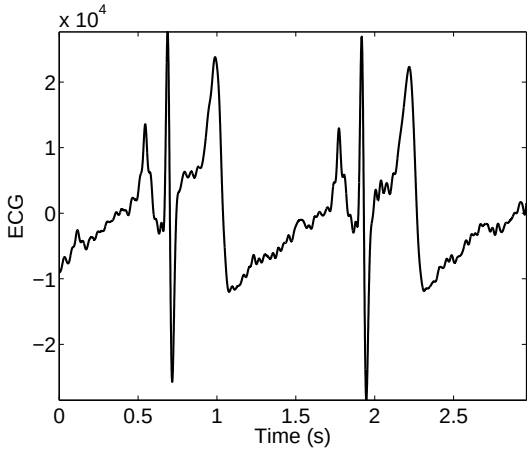

(b)

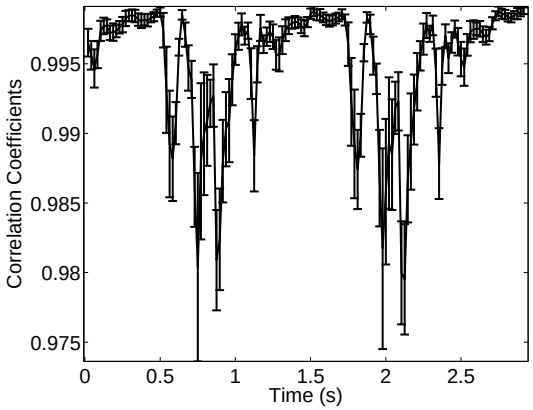

(c)

Figure 2. (a) Tracked cardiovascular-induced displacements, (b) matched ECG, and (c) average correlation coefficients. Data points in (a) and (c) indicate the mean within the ROI and error bars indicate plus and minus one standard deviation.

volume rates, expected values were calculated by decimating cumulatively-summed

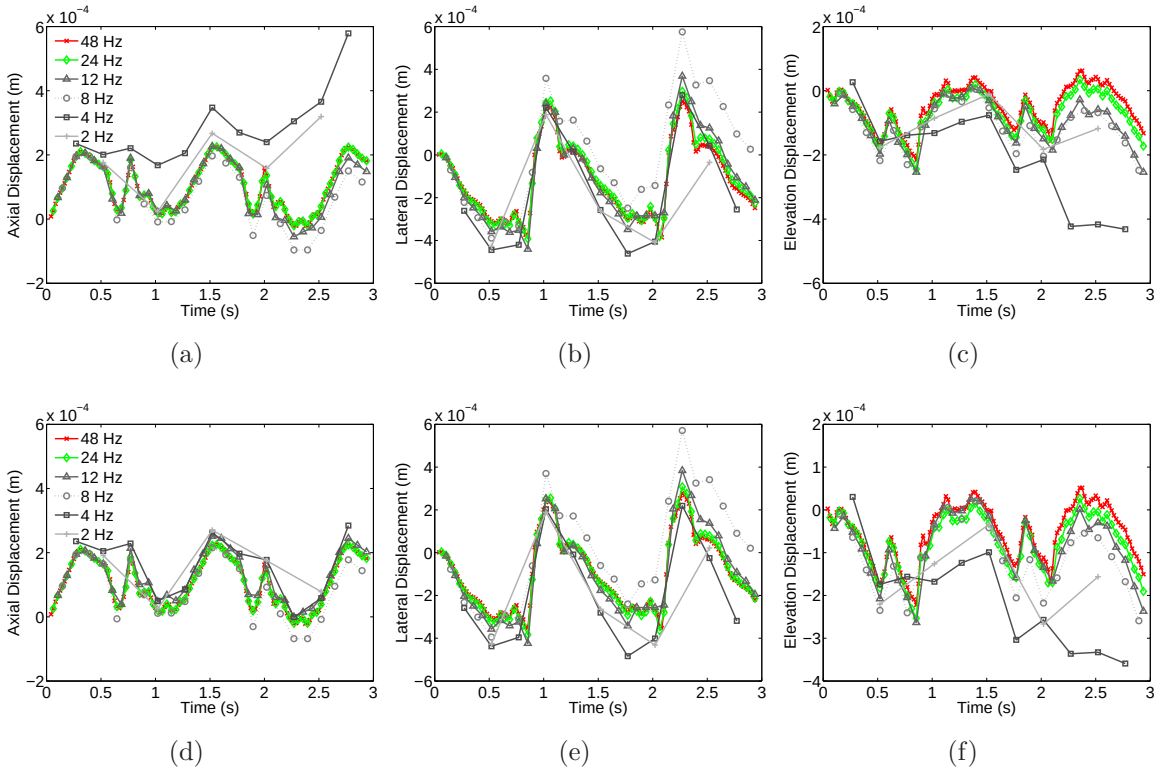

Figure 3. Tracked cardiovascular-induced displacements for the volume rates shown in the legend. The top and bottom rows respectively show displacement estimates before and after a median filter was applied to displacement maps. The axial, lateral, and elevation displacement components are shown from left to right respectively.

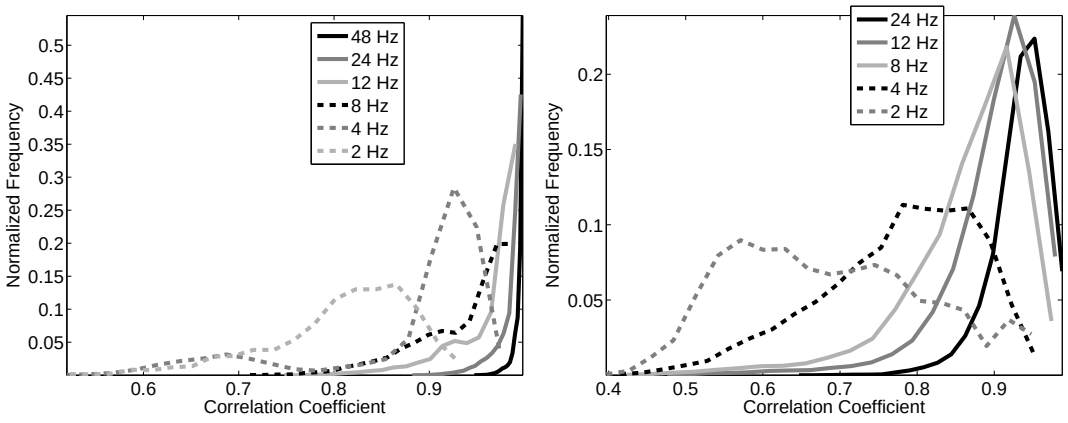

Figure 4. Histograms of the correlation coefficient between tracked kernels and their best match in corresponding search regions for the various volume rates of (a) cardiovascular-induced and (b) respiratory-dominated liver motion data for Volunteer 1. Lower correlation coefficients were calculated at the lower volume rates.

displacement results obtained at the 48 Hz volume rate. A comparison of expected and tracked results at 2 Hz is shown in Fig. 6 (a). In this example, expected and

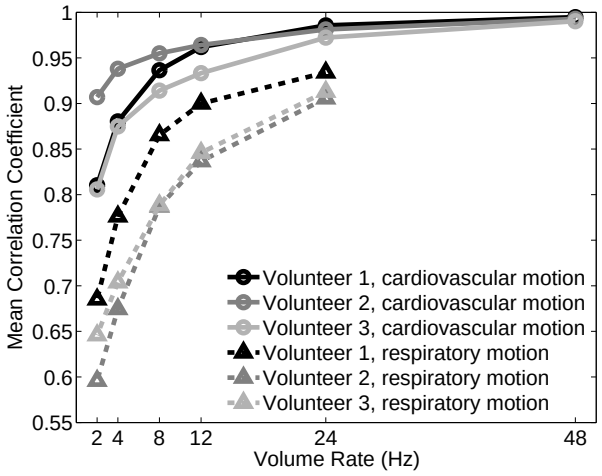

Figure 5. Mean correlation coefficients within the same 3D ROIs used to estimate displacements for all available time points, as a function of volume rate in cardiovascular-induced and respiratory-dominated liver motion data. The mean correlation coefficient decreases as the volume rate decreases.

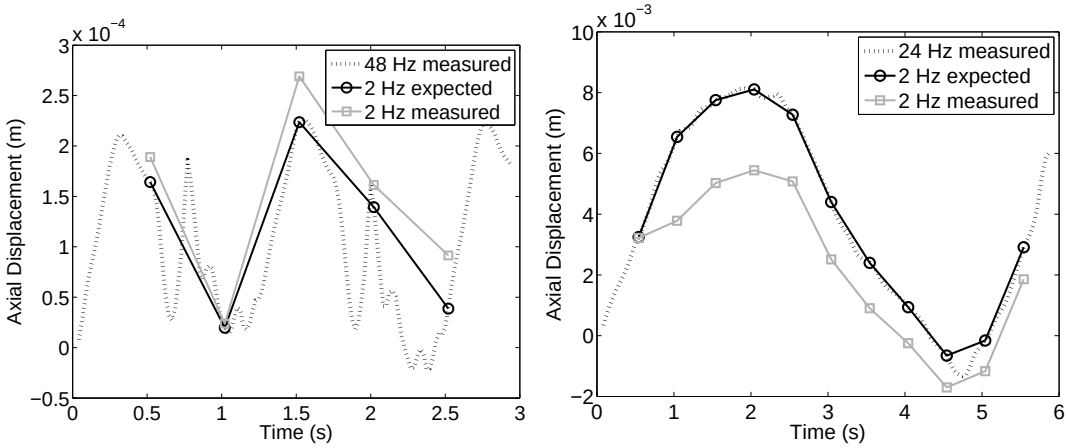

(a) (b)

Figure 6. Comparison of measured and expected values at 2 Hz for (a) cardiovascular-induced motion and (b) respiratory-dominated motion. These results were measured using median-filtered axial displacement data from Volunteer 1.

tracked results are within 0.05 mm agreement. It is also clear from this example that 2 Hz is inadequate to sample frequencies of cardiac-induced liver motion.

The deviation of tracked displacements at lower volume rates from tracked displacements at the initial 48 Hz volume rate was measured via the root mean squared deviation (RMSD). Figure 7 shows this result for the three volunteers, in each of the three dimensions, calculated with data from pre- and post-median filtered displacement maps. Unfiltered 48 Hz estimates serve as the reference for unfiltered results while median-filtered 48 Hz estimates serve as the reference for filtered results. The RMSD generally increases as volume rate is decreased. Median filtering lowers the RMSD in

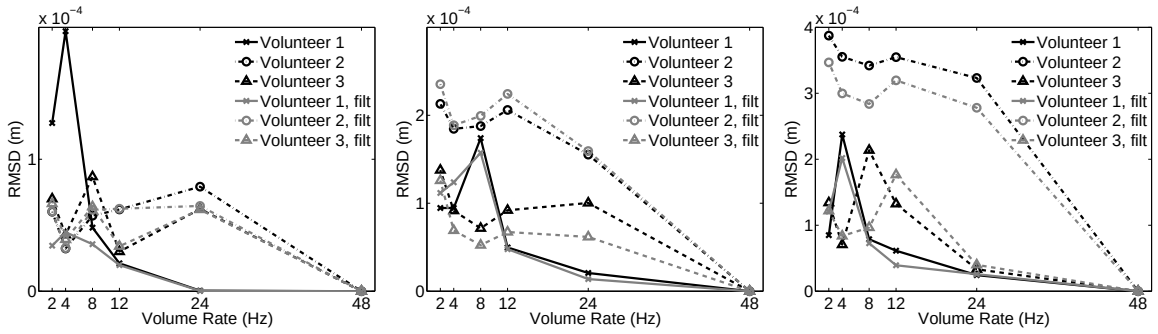

Figure 7. Root mean squared deviation (RMSD) from tracked estimates at 48 Hz in (a) axial, (b) lateral, and (c) elevation dimensions of cardiac-induced liver motion. Median filtering (denoted as filt) lowers the RMSD in most cases.

most cases.

3.2. Respiratory-dominated motion

Median-filtered displacement estimates during free breathing are shown in Figure 8 for the three volunteers, as a function of time. The MAD between median-filtered and unfiltered displacements ranged from 0.06-0.9 mm. Results are displayed for tracked estimates at the initial 24 Hz volume rate and for tracked estimates after the omission of relevant volumes to achieve lower volume rates. The axial, lateral, and elevation displacement components are shown in the columns, from left to right respectively. Displacement estimates at the initial 24 Hz volume rate are in good agreement with lower volume rates, and tracking appears adequate at volume rates of 4-8 Hz and above for Volunteer 1 (top row) and 12-24 Hz for Volunteers 2 and 3 (middle and bottom rows, respectively). At 24 Hz, average correlation coefficients within the ROI were greater than 0.85 for all volunteers (see Figure 5) with insignificant temporal variation.

Similar to results obtained without respiratory motion, as the volume rate was decreased, intervolume displacements were greater, as expected. Although not shown, the spatial variation within displacement maps also increased with decreased volume rates. Figure 4 (b) shows the histograms of correlation coefficients within the same ROI used to average intervolume displacements in respiratory-dominated motion data from Volunteer 1. Figure 5 shows the mean correlation between tracked volumes within the same ROI, as a function of volume rate for each volunteer. Both figures indicate a decrease in correlation with decreasing volume rates. Furthermore, the correlation coefficients observed for respiratory-dominated liver motion were lower than those for cardiovascular-induced liver motion

A comparison of expected and measured displacements at the 2 Hz volume rate is shown in Figure 6 (b). Expected values were calculated by decimating cumulatively-summed displacement results obtained at the 24 Hz volume rate. The measured values are lower than expected, particularly around the peak. These lower values are

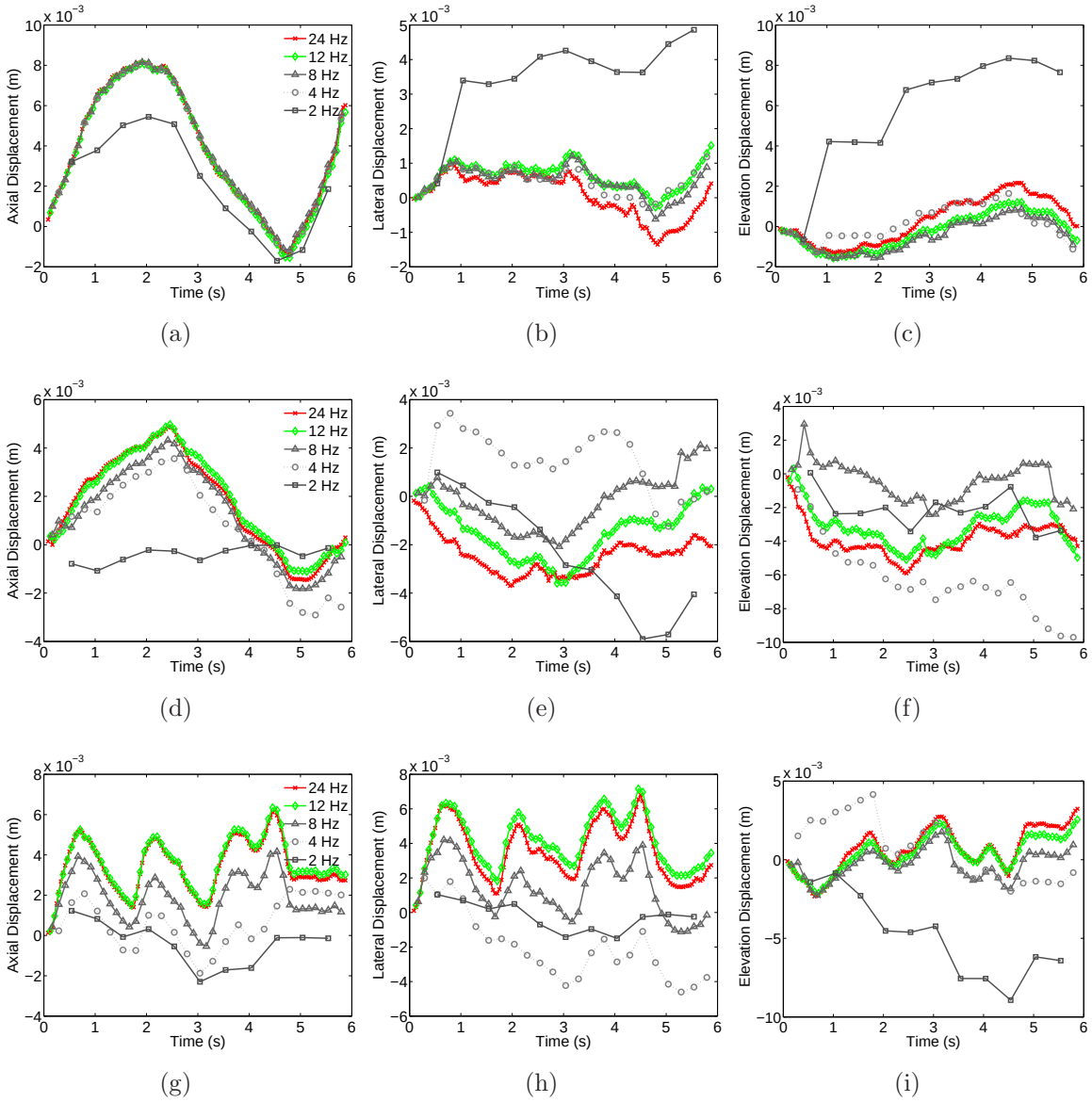

Figure 8. Respiratory-dominated tracked displacements with decreased volume rates. The three rows show median-filtered displacement estimates for Volunteers 1, 2, and 3, from top to bottom, respectively. The axial, lateral, and elevation displacement components are shown in the columns, from left to right respectively.

predominantly due to one bad estimate within the high-velocity region.

Figure 9 shows scatter plots of expected and measured velocities for all volume rates, calculated with median-filtered data. The three rows, from top to bottom, correspond to results from Volunteers 1, 2, and 3, respectively. The three columns, from left to right, correspond to results in the axial, lateral, and elevation dimensions, respectively. These results reveal that displacement estimates are generally in good agreement with the exception of a few bad estimates (i.e. estimates that largely deviate from the ideal 1:1 relationship between expected and measured values). If these bad estimates could be removed or corrected, tracking with lower volume rates would be improved. Otherwise,

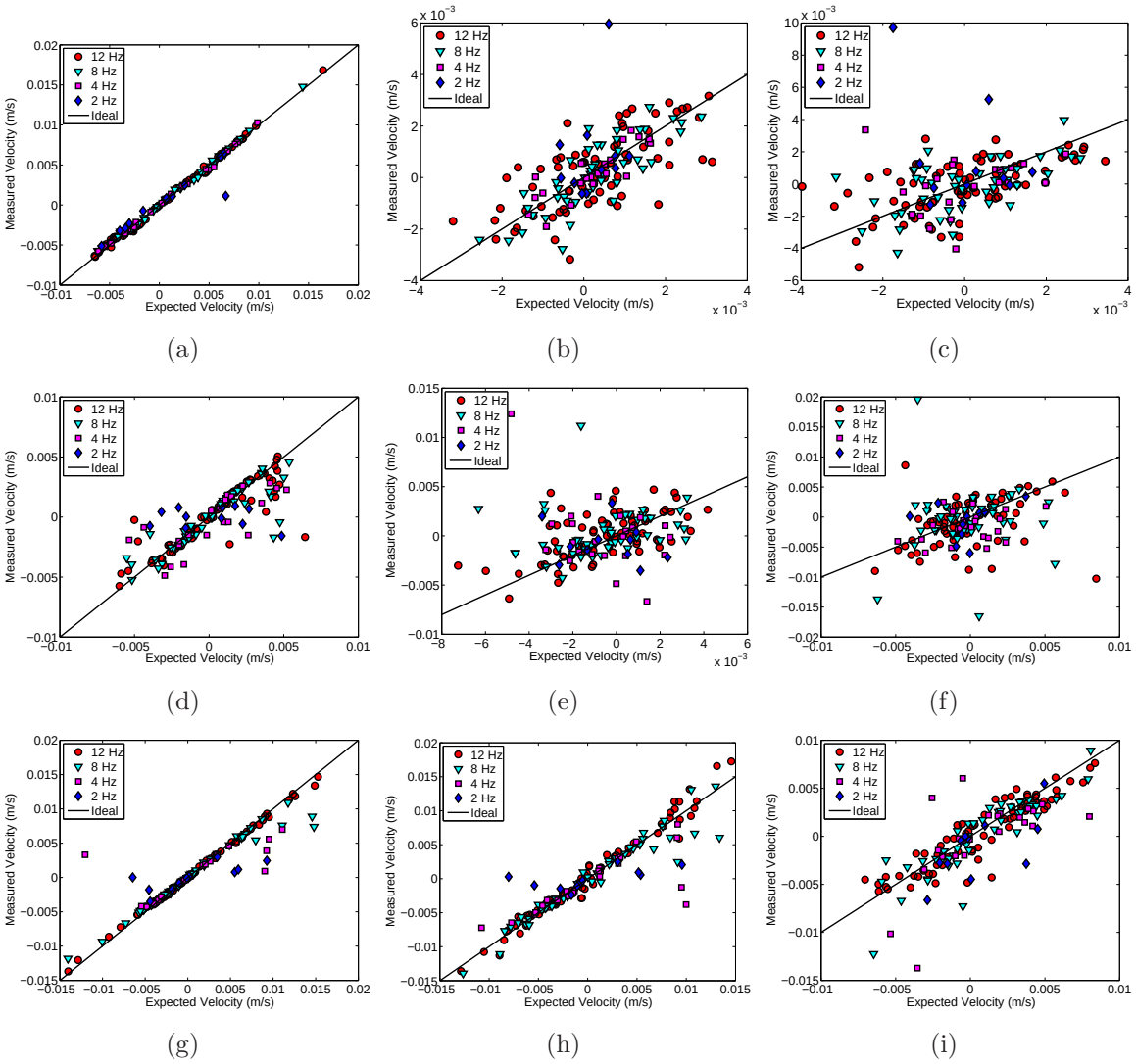

Figure 9. Scatter plots of expected and measured velocities during free breathing, for the volume rates indicated in the legend. The three rows, from top to bottom, correspond to results from Volunteers 1, 2, and 3, respectively. The three columns, from left to right, correspond to results in the axial, lateral, and elevation dimensions, respectively.

these bad estimates are expected to raise RMSD measurements.

The RMSD between tracked displacements at 24 Hz and tracked displacements at lower volume rates are displayed in Figure 10 for each volunteer. Results before and after application of a 2D median filter are shown. Filtered and unfiltered 24 Hz estimates were the reference for filtered and unfiltered results, respectively. The median filter lowers RMSD values by at most 1.7 mm. In some cases, the median filter raises RMSD estimates. Otherwise, filtered and unfiltered results are fairly similar. The RMSD generally increases with decreasing volume rates and values less than or close to 1mm are achieved at volume rates of 8-12 Hz in the three volunteers. Volunteer 1 performs the best, showing RMSD values well below 1 mm for volume rates of 4 Hz and above.

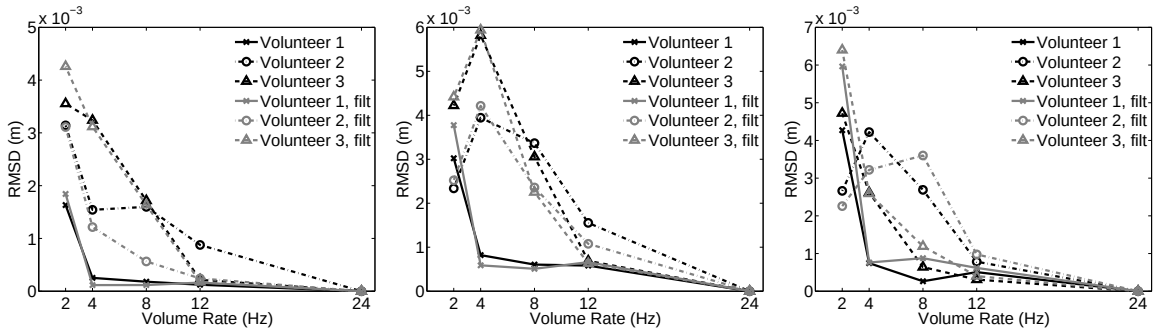

Figure 10. Root mean squared deviation from tracked estimates at 24 Hz in (a) axial, (b) lateral, and (c) elevation dimensions of respiratory-dominated liver motion. Median filtering (denoted as filt) lowers the RMSD in some cases.

These RMSD values are notably larger than those obtained for cardiovascular-induced motion.

4. Discussion

While IMRT is primarily administered during free breathing, tracking liver motion during breathhold has greatest implications for motion-compensated strategies such as such as active breathing control and gated therapy. This type of tracking also lends insight into the nature of cardiovascular-induced displacements and elucidates the relationship between spatial variation and correlation coefficients. For example, in Figure 1 (e-f), the spatial variations observed during periods of increased cardiac activity illustrate rotation, translation, and deformation of liver tissue. These three types of tissue transformations are common sources of decorrelation in ultrasonic speckle tracking (Bamber et al. 1996, Meunier 1998, Trahey et al. 1986). As noted, the transformations and associated spatial variations were more prevalent during periods of heightened cardiac activity.

During these periods, lower correlation coefficients were also observed, as demonstrated in Figure 2, and they can be explained by the greater tissue transformations that occur in the liver when cardiac activity is at its peak. Similarly, the decreased correlation at lower volume rates, shown in Figures 4 and 5, may be attributed to increased intervolume tissue transformations. Decreased correlation can result in poorer tracking performance, confirming the hypothesis that intervolume tissue transformations must be kept at a minimum by using high-enough volume rates.

Figure 3 demonstrates that volume rates greater than 8-12 Hz are needed to reliably use ultrasound data obtained with the configuration described in Section 2 to track liver motion due to cardiovascular activity. Note that the lower volume rates show poor agreement with expected values before the median filter was applied, indicating that lower volume rates produce erroneous results that have the potential to be corrected

via filtering methods. Despite filtering attempts, tracked displacements at 2 and 4 Hz show inadequate sampling of the temporal displacement waveform, as demonstrated in Figure 6 (a).

The volume rate limit for tracking cardiac-induced displacements is highly influenced by the frequency components of liver motion due to cardiac activity. Shirato et al. (2004) measured liver motion frequencies of 0.9 ± 0.2 Hz due to the beating heart in nine volunteers (not including the smaller-amplitude, higher-frequency components localized near the QRS complex which are of lesser importance for motion-compensated therapy due to their relatively small displacement scale). Practical applications of the Nyquist Theorem suggest a minimum volume acquisition speed of approximately 9 Hz to realistically sample periodicity for motion-compensated therapy, which agrees with results displayed in Figure 3 as well as with comparable results for all volunteers. In addition to inadequately-sampled cardiovascular-induced motion, lower volume rates have larger RMSD values (Figure 7), indicating increased tracking error at the lower volume rates. With regard to radiation therapies that rely on cardiac-induced motion tracking, the volumetric scan rate should at least be fast enough to sample the frequencies of cardiac motion in the area of interest. The resulting information could be used in lieu of fluoroscopy tracking measurements to eliminate the surgical costs associated with fluroscopic markers and the associated radiation doses to patients.

In respiratory-dominated motion, cumulatively-summed displacements estimated with lower volume rates usually show smaller peak or trough amplitudes when compared to measurements at higher volume rates and corresponding expected values, as demonstrated in Figure 6 (b). The lower estimates are considered inaccurate by comparison and are primarily due to isolated tracking estimates that substantially deviate from expected values and influence all subsequent tracked displacements. A comparison of Figure 8 with Figure 9 demonstrates how a few bad estimates can cause large departures in the cumulatively-summed data (e.g. compare Figure 9 (a) with Figure 8 (a)). Another example of this is observed by comparing the 12 Hz and 8 Hz results of Figures 8 (g) and 9 (g)), where the few bad estimates in the high-velocity region of the 8Hz data accumulate to give a displacement estimate at 5.5s that differs by 2mm. This behavior of the incremental tracking method has been noted in previous work (Bamber et al. 1996, Harris et al. 2010, Harris et al. 2011).

Displacement profiles that agree with estimates achieved at high volume rates are used to identify suitable volume rate limits for tracking respiratory-dominated liver motion. Displacement estimates obtained with low volume rates are corrupted by speckle decorrelation, even if temporal resolution is good enough to resolve the frequencies of motion. Results from three volunteers indicate that a minimal volume rate of 8-12 Hz is needed to achieve RMSD values less than or close to 1 mm, as shown in Figure 10. The exact volume rate limit varies with each volunteer and with acceptable RMSD threshold values, which should be based on knowledge of tracking limitations (discussed below).

There are several sources of error with this tracking method. First, incremental 3D

tracking suffers from an accumulation of tracking error, as noted previously. Secondly, false peaks and jitter are common sources of error in speckle tracking (Ramamurthy & Trahey 1991, Walker & Trahey 1995, Akiyama et al. 1988, Meunier 1998, Trahey et al. 1986). Jitter occurs when the peak of a correlation function is shifted due to electronic noise, decorrelation, and other factors, placing an uncorrectable lower bound on tracking accuracy. Byram et al. (2010) have demonstrated with tissue-mimicking phantom studies that the error of our 3D tracking algorithm is within expected jitter magnitudes, ranging from 0.1 to 1 mm in lateral and elevational dimensions and significantly less than 0.1 mm in the axial dimension. These expected jitter magnitudes dictate the minimum accuracy of the scatter plots in Figure 9. However errors of 0.1-1.0 mm are well within the range acceptable for radiotherapy treatment set-up and are comparable to fluoroscopy tracking errors (Shirato et al. 2000). Note that correlation coefficients are lower and RMSD values are greater for the respiratory-dominated 4-8 Hz volume rates of Volunteers 2 and 3 (compared to those of Volunteer 1). This is likely due to the larger displacements and velocities in the respiratory-dominated liver motion for these volunteers, particularly in the lateral and elevation dimensions where jitter in tracking estimates is greatest. The accumulation of error further increases the RMSD values for these volunteers. A third source of error is the spatial averaging of displacements within an ROI, which could introduce errors due to spatial variation, particularly at lower volume rates where increased intervolume tissue transformations are expected. However, 3D spatial averaging has the advantage of reducing noise artifacts in tracking estimates. These sources of tracking error should be considered when selecting appropriate RMSD threshholds and designing PTV margins for each patient.

Isolated tracking errors were mitigated by applying a 2D median filter to displacement maps. In most cases, the median filter reduced deviations between higher and lower volume rates, while maintaining comparable unfiltered values at the higher volume rates, as demonstrated in Figure 3. As a result of the median filter, lower RMSD values were achieved in most cases.

The scatter plots in Figure 9 indicate that a more robust error detection, correction, and/or rejection scheme has the potential to further improve tracking estimates. Such improvements are especially necessary when scanning time is increased, given the previously-discussed accumulation of tracking error. Improvements are possible by considering the motion of adjacent pixels in the three spatial dimensions (i.e. axial, lateral, and elevation) and in the temporal dimension, and coupling that information with knowledge of the spatiotemporal continuity of liver tissue. The 2D median filter employs this concept. A more refined approach is expected to improve tracking results, yet the study of such methods is beyond the scope of this paper.

The availability of 4D ultrasound scanners with matrix array transducers and parallel receive beamforming offers increased opportunity to track tissue at higher volume rates than previously possible. This is the first study to use such a system to track 4D liver displacements at volume rates as high as 48 Hz. Although analyses

were performed off-line, real-time speckle tracking has been implemented in a variety of commercial 2D and 3D ultrasound systems for the purposes of elastography (Treece et al. 2008, Lindop et al. 2008) and should therefore be feasible in the context of radiotherapy guidance. Buffer size does not pose a limitation to clinically-relevant tracking time durations if data is not stored on the scanner's hardware.

The presented approach of tracking average displacements within a ROI could be useful for guiding IMRT if the ROI is placed within a treatment PTV to monitor when cumulatively-summed liver displacements in any dimension exceeds a certain percentage of the PTV in that dimension. Ideally, the ROI and the focal depth would be in the same region since there are advantages (e.g. better resolution and signal-to-noise ratios, less jitter) to tracking near the focus (Nightingale et al. 2002).

5. Conclusion

This study utilized a 4D ultrasound system and 2D matrix array to demonstrate that volume rates as high as 8-12 Hz are needed to estimate cardiovascular-induced and respiratory-dominated liver motion with 3D ultrasound speckle tracking. Displacement estimates obtained with lower volume rates were shown to be corrupted by the undersampling of cardiovascular-induced motion and speckle decorrelation. Volume acquisition rates within this range should be employed for effective ultrasound-guided motion compensation during IMRT with this type of imaging system. The absolute limit may vary with each patient.

Acknowledgements

The authors are grateful to Siemens Medical Solutions, Inc. USA, Ultrasound Division for in-kind support. This work was supported by a Whitaker International Fellowship from the Institute of International Education.

References

Akiyama I, Nakajima N & Yuta S 1988 'Movement analysis using B-mode images' *Acoust Imaging* **17**, 499–505.

Balter J, Ten Haken R, Lawrence T, Lam K & Robertson J 1996 'Uncertainties in CT-based radiation therapy treatment planning associated with patient breathing* 1' *International Journal of Radiation Oncology* Biology* Physics* **36**(1), 167–174.

Bamber J, Verwey J, Eckersley R, Hill C & ter Haar G 1996 'Potential for tissue movement compensation in conformal cancer therapy' *Acoustical imaging* p. 239.

Bouchet L, Meeks S, Goodchild G, Bova F, Buatti J & Friedman W 2001 'Calibration of three-dimensional ultrasound images for image-guided radiation therapy' *Physics in Medicine and Biology* **46**(2), 559–578.

Byram B, Holley G, Giannantonio D & Trahey G 2010 '3-D Phantom and In Vivo Cardiac Speckle Tracking Using a Matrix Array and Raw Echo Data' *IEEE transactions on ultrasonics, ferroelectrics, and frequency control* **57**(4), 839–854.

Case R, Moseley D, Sonke J, Eccles C, Dinniwell R, Kim J, Bezjak A, Milosevic M, Brock K & Dawson L 2010 'Interfraction and Intrafraction Changes in Amplitude of Breathing Motion in Stereotactic Liver Radiotherapy' *International Journal of Radiation Oncology* Biology* Physics* .

Davies S, Hill A, Holmes R, Halliwell M & Jackson P 1994 'Ultrasound quantitation of respiratory organ motion in the upper abdomen' *British journal of radiology* **67**(803), 1096.

Dawson L, Brock K, Kazanjian S, Fitch D, McGinn C, Lawrence T, Ten Haken R & Balter J 2001 'The reproducibility of organ position using active breathing control (ABC) during liver radiotherapy' *International Journal of Radiation Oncology* Biology* Physics* **51**(5), 1410–1421.

Doyley M, Bamber J, Fuechsel F & Bush N 2001 'A freehand elastographic imaging approach for clinical breast imaging: system development and performance evaluation' *Ultrasound in medicine & biology* **27**(10), 1347–1357.

Eccles C, Brock K, Bissonnette J, Hawkins M & Dawson L 2006 'Reproducibility of liver position using active breathing coordinator for liver cancer radiotherapy' *International Journal of Radiation Oncology* Biology* Physics* **64**(3), 751–759.

Embree P 1986 ' The accurate ultrasonic measurement of the volume flow of blood by time domain correlation'.

Frey G & Chiao R 2008 '4z1c real-time volume imaging transducer' *Siemens Healthcare Sector, White Paper, 2008* .

Geiman B, Bohs L, Anderson M, Breit S & Trahey G 2000 'A novel interpolation strategy for estimating subsample speckle motion' *Physics in Medicine and Biology* **45**(6), 1541–1552.

Harris E, Miller N, Bamber J, Evans P & Symonds-Tayler J 2007 'Performance of ultrasound based measurement of 3D displacement using a curvilinear probe' *Physics in Medicine and Biology* **52**, 5683–5703.

Harris E, Miller N, Bamber J, Symonds-Tayler J & Evans P 2010 'Speckle tracking in phantom and feature-based tracking in liver in the presence of respiratory motion using 4D ultrasound' *Physics in Medicine and Biology* .

Harris E, Miller N, Bamber J, Symonds-Tayler J & Evans P 2011 'The effect of object speed and direction on the performance of 3d speckle tracking using a 3d swept-volume ultrasound probe' *Physics in Medicine and Biology* **56**, 7127.

Hsu A, Miller N, Evans P, Bamber J & Webb S 2005 'Feasibility of using ultrasound for real-time tracking during radiotherapy' *Medical physics* **32**, 1500.

Kitamura K, Shirato H, Seppenwoolde Y, Shimizu T, Kodama Y, Endo H, Onimaru R, Oda M, Fujita K, Shimizu S et al. 2003 'Tumor location, cirrhosis, and surgical history contribute to tumor movement in the liver, as measured during stereotactic irradiation using a real-time tumor-tracking radiotherapy system* 1' *International Journal of Radiation Oncology* Biology* Physics* **56**(1), 221–228.

Kubo H & Hill B 1996 'Respiration gated radiotherapy treatment: a technical study' *Physics in medicine and biology* **41**, 83.

Langen K & Jones D 2001 'Organ motion and its management' *International Journal of Radiation Oncology* Biology* Physics* **50**(1), 265–278.

Lindop J, Treece G, Gee A & Prager R 2008 'An intelligent interface for freehand strain imaging' *Ultrasound in medicine & biology* **34**(7), 1117–1128.

Mageras G & Yorke E 2004 *in* 'Seminars in Radiation Oncology' Vol. 14 Elsevier pp. 65–75.

Meunier J 1998 'Tissue motion assessment from 3D echographic speckle tracking' *Physics in Medicine and biology* **43**, 1241.

Murphy M, Balter J, Balter S, BenComo Jr J, Das I, Jiang S, Ma C, Olivera G, Rodebaugh R, Ruchala K et al. 2007 'The management of imaging dose during image-guided radiotherapy: Report of the AAPM Task Group 75' *Medical physics* **34**, 4041.

Nightingale K, Soo M, Nightingale R & Trahey G 2002 'Acoustic radiation force impulse imaging: in vivo demonstration of clinical feasibility' *Ultrasound in medicine & biology* **28**(2), 227–235.

O'Donnell M, Skovoroda A, Shapo B & Emelianov S 1994 'Internal displacement and strain imaging using ultrasonic speckle tracking' *Ultrasonics, Ferroelectrics and Frequency Control, IEEE Transactions on* **41**(3), 314–325.

Ramamurthy B & Trahey G 1991 'Potential and limitations of angle-independent flow detection algorithms using radio-frequency and detected echo signals' *Ultrasonic imaging* **13**(3), 252–268.

Shirato H, Seppenwoolde Y, Kitamura K, Onimura R & Shimizu S 2004 *in* 'Seminars in Radiation Oncology' Vol. 14 Elsevier pp. 10–18.

Shirato H, Shimizu S, Kitamura K, Nishioka T, Kagei K, Hashimoto S, Aoyama H, Kunieda T, Shinohara N, Dosaka-Akita H et al. 2000 'Four-dimensional treatment planning and fluoroscopic real-time tumor tracking radiotherapy for moving tumor* 1' *International Journal of Radiation Oncology* Biology* Physics* **48**(2), 435–442.

Suramo I, Päivänsalo M & Myllylä V 1984 'Cranio-caudal movements of the liver, pancreas and kidneys in respiration.' *Acta radiologica: diagnosis* **25**(2), 129.

Trahey G, Smith S & Von Ramm O 1986 'Speckle pattern correlation with lateral aperture translation: Experimental results and implications for spatial compounding.' *IEEE TRANS. ULTRASONICS FERROELECT. FREQ. CONTROL.* **33**(3), 257–264.

Treece G, Lindop J, Gee A & Prager R 2008 'Freehand ultrasound elastography with a 3-d probe' *Ultrasound in medicine & biology* **34**(3), 463–474.

Ustuner K 2008 'High information rate volumetric ultrasound imaging' *Siemens Healthcare Sector, White Paper* .

von Siebenthal M, Székely G, Lomax A & Cattin P 2007 'Systematic errors in respiratory gating due to intrafraction deformations of the liver' *Medical physics* **34**, 3620.

Walker W & Trahey G 1995 'A fundamental limit on delay estimation using partially correlatedspeckle signals' *IEEE Transactions on Ultrasonics, Ferroelectrics and Frequency Control* **42**(2), 301–308.

Wear K 1987 'Theoretical analysis of a technique for the characterization of myocardium contraction based upon temporal correlation of ultrasonic echoes.' *IEEE TRANS. ULTRASONICS FERROELECTR. FREQ. CONTROL.* **34**(3), 368–375.

Wurm R, Gum F, Erbel S, Schlenger L, Scheffler D, Agaoglu D, Schild R, Gebauer B, Rogalla P, Plotkin M et al. 2006 'Image guided respiratory gated hypofractionated stereotactic body radiation therapy (h-sbrt) for liver and lung tumors: Initial experience' *Acta Oncologica* **45**(7), 881–889.